Preprints of the 19th World Congress
The International Federation of Automatic Control
Cape Town, South Africa. August 24-29, 2014

Adaptive predictive control of transient vibrations of cantilevers with changing weight ⋆

Gergely Takács * **Tomáš Polóni** ** **Boris Rohaľ-Ilkiv** ***

* *Faculty of Mechanical Engineering, Slovak University of Technology, Bratislava 812 31, Slovakia (Tel: +421-907-165-720; e-mail: gergely.takacs@stuba.sk).*
** ∼,*(e-mail: tomas.poloni@stuba.sk)*
*** ∼,*(e-mail: boris.rohal-ilkiv@stuba.sk)*

Abstract: A method to control the transient vibrations in cantilever beam structures with variable weight is presented. The proposed adaptive approach is based on the hybrid extended Kalman filter (EKF) for the joint estimation of dynamic states and the weight parameter, in combination with dual-mode infinite horizon model predictive control (MPC). This adaptive predictive method is compared to nominal linear quadratic (LQ) control and positive position feedback (PPF) in experiment. Experiments are performed on an active cantilever beam with piezoelectric actuation, subjected to transient vibration effects and weight variations. The results presented in this article suggest that the proposed algorithm outperforms its traditional counterparts, while requiring less inputs to the actuated structure.

1. INTRODUCTION

Vibrations are omnipresent in engineering disciplines, as movement—and mechanical action in general—is often accompanied by the phenomenon of oscillations. Since in the majority of cases these vibrations are undesired and decrease the performance and even the safety of systems and structures, a great effort is invested in their minimization. The once passive-only approaches are today complemented by more effective, but also more complicated semi-active and active vibration control (AVC) methods [Inman, 2006].

Although simple in nature, the dynamic behavior of fixed–free cantilever beams may represent a class of real-life structures such as aircraft wings and helicopter rotors. The temporal vibration response of fixed–free beams is of special interest, as according to Richelot et al. [2004] it emulates the transient behavior typical for aerospace constructions. In addition to standard passive measures, active vibration control methods such as positive position feedback (PPF) and linear quadratic (LQ) control combined with some kind of actuation have emerged from academic deliberations into real-world applications [Unger et al., 2013]. This article deals with the active transient vibration control of mechanical structures subject to weight changes, which is often the case with aircraft wing surfaces (amount of fuel and payload changes).

The method proposed here for the adaptive control of transient vibrations in cantilevers lies in the joint estimation of dynamic states and the equivalent weight as an unknown parameter using the extended Kalman filter (EKF) [Simon, 2006], combined with dual-mode model predictive control (MPC) with the ability to handle process constraints imposed on actuator inputs [Rossiter, 2003]. Even though both of these methods have been around for decades, their combination into an adaptive control scheme is not common in literature. The novelty of this article therefore does not lie in a theoretical contribution, rather in applying the combination of two well-established methods to create a new algorithm for a particular application area and contrasting its merits with traditional methods in experiment.

The traditional approach to handle operating point change in any controlled plant is robust and adaptive control, with all the established advantages and disadvantages of these methods. This is also valid for the active control of vibrations, where robust PPF [Song et al., 2002], LQ [Hu and Ng, 2005] and other approaches are widespread. On the other side, adaptive control designs in vibration control feature self-tuning minimum variance control [Zhang et al., 2013], model reference adaptive control (MRAC) [Trajkov et al., 2008] and others. Literature research reveals that the use of EKF for vibration control is centered mainly on parameter or disturbance force identification [Lourens et al., 2012] and structural diagnostics [Mu et al., 2013], however, in the work of Szabat and Orlowska-Kowalska [2008] the role of EKF shifts from the background to serve as the means of online identification for adaptive control.

In this article, the simplified dynamic model of a cantilever beam considered in the hybrid EKF formulation is augmented by the unknown equivalent mass parameter and a shaping filter, rendering the otherwise linear dynamic model to a nonlinear estimation problem. The estimated mass is pre-filtered, then passed into the adaptive dual-

⋆ This work has been supported by the Slovak Research and Development Agency (APVV) under the contracts APVV-0090-10, APVV-0131-10, APVV 0280-06 and by the Scientific Grant Agency (VEGA) of the Ministry of Education, Science, Research and Sport of the Slovak Republic under the contract 1/0138/11.

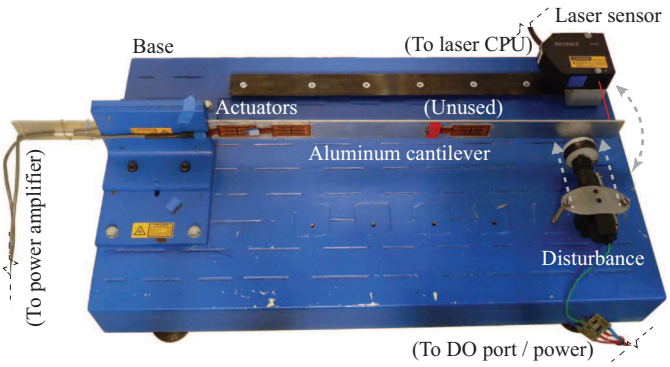

Fig. 1. Photograph of the experimental system

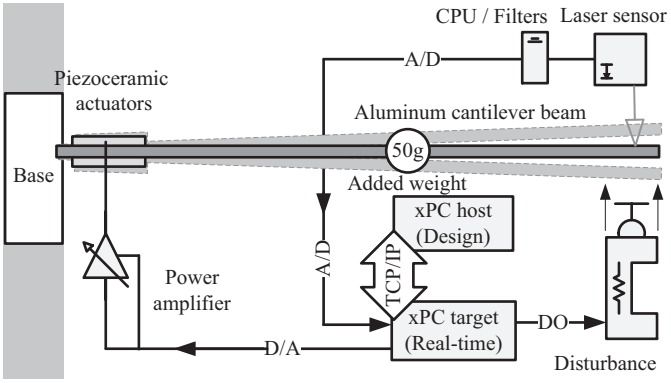

Fig. 2. Connection schematics of the experimental system

mode infinite horizon MPC formulation. The resulting adaptive EKF-MPC is tested experimentally on an active cantilever with piezoceramic actuation, subjected to repeated transient vibration events initiated by an impact mechanism emulating release tests. The experiment consists of an initial open-loop identification stage with different EKF configuration, which is followed by a control stage with the original beam and the beam with its weight modified while in operation. The adaptive EKF-MPC algorithm is compared to the positive position feedback and linear quadratic control methods that are widely accepted for the active control of transient vibrations. It is ensured that the tuning of the PPF and LQ controllers is analogous to the investigated EKF-MPC algorithm for the nominal beam configuration. The superimposed output and input responses for all tested controllers is complemented by a performance analysis.

2. EXPERIMENTAL HARDWARE

An aluminum blade measuring 550×40×3 mm is fixed in a cantilever beam configuration, with one fixed and one free end (Fig. 1). The beam is equipped by MIDÉ QP16n piezoceramic actuators that are placed close to the fixed end in order to maximize the bending moment in the first resonant mode. The actuators are driven through a MIDÉ EL-1225 capacitive operational amplifier with a 20× gain. The position of the beam is measured at the free end using a Keyence LK-G 82 laser triangulation system, connected to a Keyence LK-G3001V processing and filtering unit. The measured output and the supplied input are analog voltage signals processed by a National Instruments PCI-6030E laboratory measurement card.

The disturbance force is delivered to the beam using a stinger mechanism driven by a linear motor. Upon receiving a digital signal, the mechanism delivers a shock-like impact to the end of the beam then returns to its starting position, leaving the beam to vibrate freely afterwards. The impacts generated by the stinger mechanism emulate the transient vibration effects common in aerospace constructions [Richelot et al., 2004] that are routinely simulated by release tests in laboratory settings [Vasques and Rodrigues, 2006, Choi et al., 1998]. In this work, the stinger mechanism is employed for the repeatable reproduction of release tests in order to enable the comparison of the proposed control strategy with nominal LQ and PPF controllers.

The control algorithms were developed in the Matlab–Simulink software environment. Offline portions of the code were initialized using the m-file scripting language. The online implementation of the algorithm combines built-in blocks with customized blocks first coded in the m-file language, then re-compiled into a C language Real-Time Workshop target code using the Embedded Matlab Editor. The Simulink control schemes were then loaded onto a personal computer containing the measurement card and running the xPC Target control system prototyping software. The connection scheme of the experimental hardware and the xPC Target and Host computers is shown in Fig. 2.

3. CONTROLLER DESIGN

3.1 System modeling

Since the first vibration mode dominates the response of the physical system, let us assume that the dynamics of the blade can be modeled using a single degree of freedom (DOF) mass-spring-damper system, which is subject to an unknown external force disturbance

$$m\ddot{q}(t) + b\dot{q}(t) + kq(t) = cu(t) + F_e(t), \tag{1}$$

where $q(t)$ is the scalar variable representing the position of the beam measured at the end, $u(t)$ is the voltage input supplied to the piezoceramic actuators and $F_e(t)$ is the external disturbance force that will be later treated as nonwhite Gaussian process noise. The equivalent mass of the beam is m (kg), the equivalent viscous damping coefficient is b (Ns/m), the spring constant is k (N/m) and the scalar force conversion constant c (N/V) represents the amount of force supplied to the blade by the actuators per unit voltage input.

Choosing the position and velocity as state variables results in the continuous linear state-space model

$$\dot{\boldsymbol{x}}(t) = \boldsymbol{\Phi}\boldsymbol{x}(t) + \boldsymbol{\Gamma}u(t) \tag{2}$$

$$y(t) = \boldsymbol{C}\boldsymbol{x}(t), \tag{3}$$

where $\boldsymbol{\Phi}$ is the $\mathbb{R}^{2\times2}$ state transition matrix, $\boldsymbol{\Gamma}$ is the $\mathbb{R}^{2\times1}$ input matrix that for the cantilever dynamics is assumed:

$$\boldsymbol{\Phi} = \begin{bmatrix} 0 & 1 \\ -\dfrac{k}{m} & -\dfrac{b}{m} \end{bmatrix} \qquad \boldsymbol{\Gamma} = \begin{bmatrix} 0 \\ \dfrac{c}{m} \end{bmatrix}. \tag{4}$$

The measured output is position only, therefore the output matrix is $\boldsymbol{C} = [1\ 0]$. All the physical parameters will be treated as unknown during the initial identification phase (marked with the subscript "I"), while parameters b, k and c will be fixed throughout the adaptive control part (marked with the subscript "C") and only the equivalent mass $m(t)$ will be treated as variable, resulting in continuously updated $\boldsymbol{\Phi}_C(t)$ and $\boldsymbol{\Gamma}_C(t)$ matrices. In case the formulation is valid for both modes, the subscript "θ" will be used:

$$\theta = \begin{cases} I & \text{if } t \leq T_i \\ C & \text{if } t > T_i, \end{cases} \tag{5}$$

where T_i is the length of the initial identification phase.

Identification mode The continuous state can be augmented by the vector of unknown parameters $\boldsymbol{p}_I(t) = [k(t)\ b(t)\ c(t)\ m(t)]^T$, where $\boldsymbol{p}_I(t)$ expresses the parameters during the initial identification phase. The system model can be expressed as

$$\dot{\boldsymbol{x}}(t) = \tilde{f}_c(\boldsymbol{x}(t), \boldsymbol{p}_I(t), u(t)) + w_s(t) \tag{6}$$
$$\dot{\boldsymbol{p}}_I(t) = w_p(t), \tag{7}$$

where quantities $w_s(t)$ and $w_p(t)$ are the system process noise and parameter process noise. Combining Eqs. (6)–(7) we obtain the new augmented state $\boldsymbol{x}_I(t) = [\boldsymbol{x}(t)\ \boldsymbol{p}_I(t)]^T$ that can be used to describe the dynamic states supplemented by the unknown parameters:

$$\dot{\boldsymbol{x}}_I(t) = f_c(\boldsymbol{x}_I(t), u(t)) + w(t) \tag{8}$$
$$y(t) = h_c(\boldsymbol{x}_I(t), u(t)) + v(t), \tag{9}$$

where the function f_c represents the continuous augmented dynamics, h_c is the continuous measurement function and $w(t) = [w_s(t)\ w_p(t)]^T$ expresses the combined system and parameter process noise. In the case of the initial identification of the blade parameters, we expect the process and measurement noise to have the properties of white Gaussian noise, that is $w(t) \sim N(0, \boldsymbol{Q}_{If})$ and $v(t) \sim N(0, \boldsymbol{R}_I)$ where the properties of the noise are described by the covariance matrices $\boldsymbol{Q}_{If}$ and $\boldsymbol{R}_I$.

Control mode The only unknown variable during the adaptive control of the blade is the estimated equivalent mass, rendering the vector of unknown parameters to $p_C(t) = m(t)$. The rest of the parameters are fixed and obtained from the initial identification. Similarly to the previous case, the state will be augmented by $m(t)$:

$$\dot{\boldsymbol{x}}(t) = \tilde{f}_c(\boldsymbol{x}(t), p_C(t), u(t)) + \eta_s(t) \tag{10}$$
$$\dot{p}_C(t) = w_p(t) \tag{11}$$

Because of the repeating shock-like nature of the disturbance the use of a white Gaussian noise during the control mode is inadequate, thus $\eta_s(t)$ here represents a nonwhite Gaussian noise. Nonwhite noise $\eta_s(t)$ can be generated using a linear shaping filter driven by a white Gaussian noise $w_s(t)$:

$$\dot{\boldsymbol{x}}_f(t) = f_f(\boldsymbol{x}_f(t), w_s(t)) \tag{12}$$
$$\eta_s(t) = \boldsymbol{x}_f(t)$$

The system dynamics augmented by the unknown mass can be further expanded by the dynamics of the linear spectrum shaping filter in Eq. (12) to obtain

$$\dot{\boldsymbol{x}}(t) = \tilde{f}_{f,c}(\boldsymbol{x}(t), p_C(t), u(t)) + \boldsymbol{x}_f(t) \tag{13}$$
$$\dot{p}_C(t) = w_p(t) \tag{14}$$
$$\dot{\boldsymbol{x}}_f(t) = f_f(\boldsymbol{x}_f(t), w_s(t)) \tag{15}$$

resulting in the state $\boldsymbol{x}_C(t) = [\boldsymbol{x}(t)\ p_C(t)\ \boldsymbol{x}_f(t)]^T$ and the corresponding dynamics summarized by

$$\dot{\boldsymbol{x}}_C(t) = f_c(\boldsymbol{x}_C(t), u(t)) + w(t) \tag{16}$$
$$y(t) = h_c(\boldsymbol{x}_{C,a,f}(t), u(t)) + v(t), \tag{17}$$

where the function f_c represents the continuous augmented dynamics, h_c is the continuous measurement function and $w(t) = [w_s(t)\ w_p(t)]^T$ expresses system and parameter process noise. The statistical properties of the process and measurement noise are contained in the covariance matrices $\boldsymbol{Q}_{Cf}$ and $\boldsymbol{R}_C$.

Despite the fact that the system dynamics is continuous, measurements can be made only in discrete time intervals, so Eqs. (8) and (16) will be propagated through numerical integration using the Euler method, resulting in discrete-time functions $f(\boldsymbol{x}_{\theta(k)}, u_{(k)})$ and $h(\boldsymbol{x}_{\theta(k)}, u_{(k)})$ in the observer.

3.2 Observer formulation

The observer considered for the estimation of system states and parameters during both the initial identification and control operation modes is known in literature as the continuous-discrete extended Kalman filter, and the formulation is based on Simon [2006] and Maybeck [1979]. The EKF algorithm is launched with the initial estimate of the state $\hat{\boldsymbol{x}}^+_{\theta(0)} = E\left[\boldsymbol{x}_{\theta(0)}\right]$ and the initial covariance of the state estimate error:

$$\boldsymbol{P}^+_{\theta(0)} = E\left[(\boldsymbol{x}_{\theta(0)} - \hat{\boldsymbol{x}}^+_{\theta(0)})(\boldsymbol{x}_{\theta(0)} - \hat{\boldsymbol{x}}^+_{\theta(0)})^T\right] \tag{18}$$

In order to obtain the a priori state estimates (denoted by the $^-$ superscript), the dynamic system in Eqs. (8) and (16) is integrated one step ahead to the next time instant: $\hat{\boldsymbol{x}}^-_{\theta(k)} = f(\hat{\boldsymbol{x}}^+_{\theta(k-1)}, u_{(k)})$.

The dynamics of the mass-spring-damper system augmented by the parameters in the case of the initial identification, assuming there are no parameter changes between sample is

$$\begin{aligned} \dot{q}(t) &= \dot{x}_{I1}(t) = x_{I2}(t) \\ \ddot{q}(t) &= \dot{x}_{I2}(t) = -x_{I6}(t)x_{I3}(t)x_{I1}(t) - x_{I6}(t)x_{I4}(t)x_{I2}(t) \\ &\quad + x_{I6}(t)x_{I5}(t)u(t) \\ \dot{k}(t) &= \dot{x}_{I3}(t) = 0 \\ \dot{b}(t) &= \dot{x}_{I4}(t) = 0 \\ \dot{c}(t) &= \dot{x}_{I5}(t) = 0 \\ \frac{1}{\dot{m}(t)} &= \dot{x}_{I6}(t) = 0. \end{aligned} \tag{19}$$

In case of online control, the only unknown parameter is weight, and the character of the process noise is different.

Assuming for simplicity that the real disturbance can be sufficiently modeled by a second-order Markov process driven by white Gaussian noise [Maybeck, 1979], the mass-spring-damper can be augmented by the unknown mass parameter and the second order state description of the shaping filter resulting in:

$$\begin{aligned}\dot{q}(t) &= \dot{x}_{C1}(t) = x_{C2}(t)\\ \ddot{q}(t) &= \dot{x}_{C2}(t) = -x_{C3}(t)x_{C1}(t)k - x_{C3}(t)x_{C2}(t)b + \\ &\quad + x_{C3}(t)cu(t) + x_{C5}(t)\\ \frac{1}{\dot{m}(t)} &= \dot{x}_{C3}(t) = 0\\ \dot{x}_{C4}(t) &= x_{C4}(t)\\ \dot{x}_{C5}(t) &= -\omega_n^2 x_{C4}(t) - 2\alpha_n x_{C5}(t),\end{aligned} \tag{20}$$

where ω_n and α_n are tuning parameters of the spectral filter and are chosen to fit the character of the real disturbance.

The time update of the a priori covariance matrix estimate is given by

$$\dot{\boldsymbol{P}}_\theta(t) = \boldsymbol{Z}_\theta(\hat{\boldsymbol{x}}_\theta(t))\boldsymbol{P}_\theta(t) + \boldsymbol{P}_\theta(t)\boldsymbol{Z}_\theta^T(\hat{\boldsymbol{x}}_\theta(t)) + \boldsymbol{Q}_{\theta f} \tag{21}$$

where the Jacobians of Eqs. (19) and (20) are defined as

$$\boldsymbol{Z}(\hat{\boldsymbol{x}}_\theta) = \left.\frac{\partial f_c(\boldsymbol{x}_\theta)}{\partial \boldsymbol{x}_\theta}\right|_{\boldsymbol{x}_\theta = \hat{\boldsymbol{x}}_\theta}. \tag{22}$$

The a priori covariance matrix estimate is obtained by the numerical propagation of Eq. (21) from sample $t = (k-1)$ to sample $t = (k)$:

$$\boldsymbol{P}^-_{\theta(k)} = g\left(\boldsymbol{P}^+_{\theta(k-1)}, \boldsymbol{Z}_\theta(\hat{\boldsymbol{x}}+_{\theta(k-1)})\right). \tag{23}$$

The discrete-time portion of the hybrid EKF algorithm is started by computing the update of the Kalman gain

$$\boldsymbol{K}_{\theta(k)} = \boldsymbol{P}^-_{\theta(k)}\boldsymbol{L}_\theta^T\left[\boldsymbol{L}_\theta\boldsymbol{P}^-_{\theta(k)}\boldsymbol{L}_\theta^T + \boldsymbol{M}_\theta\boldsymbol{R}_\theta\boldsymbol{M}_\theta^T\right]^{-1}. \tag{24}$$

The state estimate augmented by the vector of unknown parameters—and in the case of the online controller the shaping filter—is then updated to obtain the a posteriori state estimate (denoted by a $^+$ superscript) based on the measurement and the gain, along with the a posteriori error covariance:

$$\hat{\boldsymbol{x}}^+_{\theta(k)} = \hat{\boldsymbol{x}}^-_{\theta(k)} + \boldsymbol{K}_{\theta(k)}\left[y_{(k)} - h(\hat{\boldsymbol{x}}^-_{\theta(k)}, u_{(k)})\right] \tag{25}$$

$$\begin{aligned}\boldsymbol{P}^+_{\theta(k)} &= \left[\boldsymbol{I} - \boldsymbol{K}_{\theta(k)}\boldsymbol{L}_\theta\right]\boldsymbol{P}^-_{\theta(k)}\left[\boldsymbol{I} - \boldsymbol{K}_{\theta(k)}\boldsymbol{L}_\theta\right]^T + \\ &\quad + \boldsymbol{K}_{\theta(k)}\boldsymbol{M}_\theta\boldsymbol{R}_\theta\boldsymbol{M}_\theta^T\boldsymbol{K}^T_{\theta(k)},\end{aligned} \tag{26}$$

where the Jacobians of the measurement equation with respect to the state and measurement noise are given as:

$$\boldsymbol{L}_{I(k)} = \left.\frac{\partial h(\boldsymbol{x}_{I(t)})}{\partial \boldsymbol{x}_{I(t)}}\right|_{\boldsymbol{x}_{I(t)} = \hat{\boldsymbol{x}}^-_{I(t)}} = \begin{bmatrix} 0 & 0\,0\,0\,0\\ x_6(t) & 0\,0\,0\,0\\ 0 & 1\,0\,0\,0\\ 0 & 0\,1\,0\,0\\ 0 & 0\,0\,1\,0\\ 0 & 0\,0\,0\,1\end{bmatrix} \tag{27}$$

$$\boldsymbol{L}_{C(k)} = \left.\frac{\partial h(\boldsymbol{x}_{C(t)})}{\partial \boldsymbol{x}_{C(t)}}\right|_{\boldsymbol{x}_{C(t)} = \hat{\boldsymbol{x}}^-_{C(t)}} = \begin{bmatrix} 0 & 0\\ 0 & 0\\ 0 & 1\\ 1 & 0\\ \omega_n^{-2\alpha_n} & 0\end{bmatrix} \tag{28}$$

$$\boldsymbol{M}_{\theta(k)} = \left.\frac{\partial h(\boldsymbol{x}_{\theta(t)})}{\partial \boldsymbol{v}_{\theta(t)}}\right|_{\boldsymbol{x}_{\theta(t)} = \hat{\boldsymbol{x}}^-_{\theta(t)}} = 1. \tag{29}$$

3.3 Updates and discretization

Updates During the control phase, the continuous system model in Eq. (2) is updated based on windowed median-filtered estimate of the equivalent weight of the beam, resulting in matrices $\boldsymbol{\Phi}_C(t)$ and $\boldsymbol{\Gamma}_C(t)$ at times $t = kT$. The weight is varied, while the rest of the physical parameters are assumed to remain constant and are based on the results of the initial identification. The discrete, linear, time-variant model including only the dynamic states $\boldsymbol{x}_{C1}$ and $\boldsymbol{x}_{C2}$ of the cantilever used in the MPC algorithm is:

$$\boldsymbol{x}_{(k+1)} = \boldsymbol{A}_{(k)}\boldsymbol{x}_{(k)} + \boldsymbol{B}_{(k)}u_{(k)} \tag{30}$$

$$y_{(k)} = \boldsymbol{C}\boldsymbol{x}_{(k)}, \tag{31}$$

where $\boldsymbol{A}_{(k)}$ is a $\mathbb{R}^{2\times 2}$ state transition matrix, $\boldsymbol{B}_{(k)}$ is a $\mathbb{R}^{2\times 1}$ input matrix and $\boldsymbol{C} = [1\ 0]$ outputs deformation.

Discretization The continuous state and input matrices $\boldsymbol{\Phi}_C(k)$ and $\boldsymbol{\Gamma}_C(k)$ updated at sample times (k) are discretized based on the widely accepted algorithm featured in Franklin et al. [1997].

3.4 Model predictive control

The model predictive control algorithm used in this work is based on the traditional infinite-horizon constrained dual-mode formulation; where in order to obtain the optimal sequence of outputs, a cost function is minimized while constraints are enforced. The MPC formulation used here is based on Maciejowski [2000] and Rossiter [2003].

The future progress of states $\overrightarrow{\boldsymbol{x}}_{(k)}$ may be predicted up to a horizon of n steps. The current state $\boldsymbol{x}_{0(k)} = \hat{\boldsymbol{x}}^+_{0(k)}$ and the vector of future inputs $\overrightarrow{\boldsymbol{u}}_{(k)}$ are recursively substituted to the state-space model in Eq. (30) to obtain the state prediction equation $\overrightarrow{\boldsymbol{x}}_{(k)} = \boldsymbol{M}_{(k)}\boldsymbol{x}_{0(k)} + \boldsymbol{N}_{(k)}\overrightarrow{\boldsymbol{u}}_{(k)}$. In this context the estimated state $\hat{\boldsymbol{x}}^+_{0(k)}$ refers only to the dynamic portion of the augmented state, excluding parameters and shaping filter states. The state prediction matrices $\boldsymbol{M}_{(k)}$ and $\boldsymbol{N}_{(k)}$ for step (k) are

$$\boldsymbol{M}_{(k)} = \begin{bmatrix}\boldsymbol{A}^0_{(k)} & \boldsymbol{A}^1_{(k)} & \dots & \boldsymbol{A}^{n-2}_{(k)} & \boldsymbol{A}^{n-1}_{(k)} & \boldsymbol{A}^n_{(k)}\end{bmatrix}^T \tag{32}$$

$$\boldsymbol{N}_{(k)} = \begin{bmatrix}\boldsymbol{0} & \boldsymbol{0} & \dots & \boldsymbol{0}\\ \boldsymbol{B}_{(k)} & \boldsymbol{0} & \dots & \boldsymbol{0}\\ \boldsymbol{A}_{(k)}\boldsymbol{B}_{(k)} & \boldsymbol{B}_{(k)} & \dots & \boldsymbol{0}\\ \vdots & \vdots & \ddots & \vdots\\ \boldsymbol{A}^{n-1}_{(k)}\boldsymbol{B}_{(k)} & \boldsymbol{A}^{n-2}_{(k)}\boldsymbol{B}_{(k)} & \dots & \boldsymbol{B}_{(k)}\end{bmatrix}. \tag{33}$$

A linear quadratic cost function formulated on the basis of the dual-mode paradigm takes the weighted contribution of states and inputs into account, assuming the use of free control moves up to the end of the horizon and fixed feedback afterwards [Scokaert and Rawlings, 1996]:

$$J_{(k)} = \sum_{i=0}^{n-1} \left(\boldsymbol{x}_{(k+i)}^T \boldsymbol{Q} \boldsymbol{x}_{(k+i)} + u_{(k+i)}^T \boldsymbol{R} u_{(k+i)} \right) + \\ + \boldsymbol{x}_{(k+n)}^T \boldsymbol{P}_{f(k)} \boldsymbol{x}_{(k+n)}, \tag{34}$$

is expressing the quality of the control at each sample (k). Algorithm behavior may be tuned by the choice of state penalization $\boldsymbol{Q} = \boldsymbol{Q}^T \geq 0$ and input penalization $\boldsymbol{R} = \boldsymbol{R}^T \geq 0$. Terminal weight $\boldsymbol{P}_{f(k)}$ is the solution of the unconstrained, infinite-horizon quadratic regulation problem at sample (k) which can be recomputed online as the solution of the discrete-time algebraic Ricatti equation (DARE):

$$\boldsymbol{A}_{(k)}^T \boldsymbol{P}_{f(k)} \boldsymbol{A}_{(k)} - \boldsymbol{P}_{f(k)} - \boldsymbol{A}_{(k)}^T \boldsymbol{P}_{f(k)} \boldsymbol{B}_{(k)} \cdot \\ \cdot (\boldsymbol{R} + \boldsymbol{B}_{(k)}^T \boldsymbol{P}_{f(k)} \boldsymbol{B}_{(k)})^{-1} \boldsymbol{B}_{(k)} \boldsymbol{P}_{f(k)} \boldsymbol{A}_{(k)} + \boldsymbol{Q} = 0 \tag{35}$$

For the online numerical solution of the DARE, we consider an eigenvalue decomposition method based on the work of Pappas et al. [1980]. First, let us define the variable $\boldsymbol{G}_{(k)} = \boldsymbol{B}_{(k)} \boldsymbol{R}^{-1} \boldsymbol{B}_{(k)}^T$ and consider the generalized eigenvalue problem in the form $\boldsymbol{Y}_{(k)} \boldsymbol{V}_{(k)} = \boldsymbol{U}_{(k)} \boldsymbol{X}_{(k)} \boldsymbol{V}_{(k)}$, where $\boldsymbol{U}_{(k)}$ is a diagonal matrix containing generalized eigenvalues and the full matrix $\boldsymbol{V}_{(k)}$ corresponds to the generalized principal vectors. Furthermore, let us define matrices $\boldsymbol{X}_{(k)}$ and $\boldsymbol{Y}_{(k)}$ as

$$\boldsymbol{X}_{(k)} = \begin{bmatrix} \boldsymbol{I} & \boldsymbol{G}_{(k)} \\ \boldsymbol{0} & \boldsymbol{A}_{(k)}^T \end{bmatrix} \qquad \boldsymbol{Y}_{(k)} = \begin{bmatrix} \boldsymbol{A}_{(k)} & \boldsymbol{0} \\ -\boldsymbol{Q} & \boldsymbol{I} \end{bmatrix}. \tag{36}$$

The solution of the generalized eigenproblem leads to the diagonal matrix $\boldsymbol{U}_{(k)}$, which can be used to identify the stable eigenvalues. Eigenvectors of $\boldsymbol{V}_{(k)}$ corresponding to these stable eigenvalues are then extracted to matrix $\boldsymbol{W}_{(k)}$ that will be used as the basis of the stable eigenspace. Partitioning $\boldsymbol{W}_{(k)}$ into two sub-matrices yields $\boldsymbol{W}_{(k)} = \begin{bmatrix} \boldsymbol{W}_{1(k)} & \boldsymbol{W}_{2(k)} \end{bmatrix}^T$, which is then utilized to compute the solution of the DARE as $\boldsymbol{P}_{f(k)} = \boldsymbol{W}_{2(k)} \boldsymbol{W}_{1(k)}^{-1}$ at each sample time.

The core of the MPC algorithm is performing the minimization of the cost defined by Eq. (34), yielding a sequence of optimal inputs at each sample time. This minimization procedure is subject to the following constraints:

$$\underline{u} \leq u_{(k+i)} \leq \overline{u}, \; i = 0, \ldots, n-1 \tag{37}$$

$$\boldsymbol{x}_{0(k)} = \boldsymbol{x}_{(k)} \tag{38}$$

$$\boldsymbol{x}_{(k+1+i)} = \boldsymbol{A}_{(k)} \boldsymbol{x}_{(k+i)} + \boldsymbol{B}_{(k)} u_{(k+i)}, \qquad i \geq 0 \tag{39}$$

$$y_{(k+i)} = \boldsymbol{C} \boldsymbol{x}_{(k+i)}, \qquad i \geq 0 \tag{40}$$

$$u_{(k+i)} = \boldsymbol{K}_{(k)} \boldsymbol{x}_{(k+i)}, \qquad i \geq n \tag{41}$$

where Eq. (37) defines constraints on the voltage input, Eq. (38) is the observed dynamic state, Eq. (39)–(40) is the discrete state-space model updated by the estimated weight, and finally Eq. (41) is the constraint that defines the terminal cost. The cost function in (34) is transformed to

$$J_{(k)} = \overrightarrow{\boldsymbol{u}}_{(k)}^T \boldsymbol{H}_{(k)} \overrightarrow{\boldsymbol{u}}_{(k)} + 2 \boldsymbol{x}_{0(k)}^T \boldsymbol{G}_{(k)}^T \overrightarrow{\boldsymbol{u}}_{(k)} + \boldsymbol{x}_{0(k)}^T \boldsymbol{F}_{(k)} \boldsymbol{x}_{0(k)} \tag{42}$$

For the variable model structure considered in this paper, $\boldsymbol{H}_{(k)}$ and $\boldsymbol{G}_{(k)}$ is evaluated online at each step (k) by

$$\boldsymbol{H}_{(k)} = \sum_{i=0}^{n-1} \boldsymbol{N}_{i(k)}^T \boldsymbol{Q} \boldsymbol{N}_{i(k)} + \boldsymbol{N}_{n(k)}^T \boldsymbol{P}_{f(k)} \boldsymbol{N}_{n(k)} + \mathcal{R} \tag{43}$$

$$\boldsymbol{G}_{(k)} = \sum_{i=0}^{n-1} \boldsymbol{N}_{i(k)}^T \boldsymbol{Q} \boldsymbol{M}_{i(k)} + \boldsymbol{N}_{n(k)}^T \boldsymbol{P}_{f(k)} \boldsymbol{M}_{n(k)}, \tag{44}$$

where i is the i-th and n is the last block row of $\boldsymbol{N}_{(k)}$ and $\boldsymbol{M}_{(k)}$, and $\mathcal{R}$ is a block matrix with the input penalty $\boldsymbol{R}$ on its main diagonal.

3.5 The Resulting Vibration Control Strategy

The on-line portion of the adaptive predictive control strategy used in this work can be summarized by the following algorithm:

Algorithm: *At each sampling instant* (k)*:*

(1) To obtain the a priori estimates propagate the state and covariance matrix in simulation.
(2) Sample the deflection $y_{(k)}$ filtered by a low-pass and running mean filter.
(3) Compute the Kalman gain $\boldsymbol{K}_{C(k)}$.
(4) Use the measurement and Kalman gain to get a posteriori state estimates $\hat{\boldsymbol{x}}_{C(k)}^+$, then update covariance matrix $\boldsymbol{P}_{C(k)}^+$.
(5) Based on the median filtered weight estimate $\hat{m}_{(k)}$, re-assemble the continuous model $\boldsymbol{\Phi}_{C(k)}$ and $\boldsymbol{\Gamma}_{C(k)}$.
(6) Discretize the system matrices $\boldsymbol{A}_{(k)}$ and $\boldsymbol{B}_{(k)}$.
(7) Use the discretized model to compute the state prediction matrices $\boldsymbol{M}_{(k)}$ and $\boldsymbol{N}_{(k)}$.
(8) Solve the discrete-time algebraic Ricatti equation through the generalized eigenvalue method to obtain terminal weighting $\boldsymbol{P}_{f(k)}$.
(9) Use the state prediction matrices to compute the cost prediction matrices $\boldsymbol{H}_{(k)}$, $\boldsymbol{G}_{(k)}$.
(10) Minimize the cost $J_{(k)}$ subject to input constraints.
(11) Apply the first element of the vector of optimal control moves $\overrightarrow{\boldsymbol{u}}_{(k)}$ to the controlled system.

4. EXPERIMENTS

The performance of the proposed adaptive EKF-MPC vibration control strategy is compared to nominal LQ control, nominal PPF control and the open-loop response resulting in four different experimental settings. Each experiment lasting 80 s was divided into 20 s intervals: an initial identification without control and disturbances, control of the nominal system, control of the system with a small weight change and a return to the nominal system. The impacts emulating transient vibration were delivered in 4 s intervals. To simulate the change of physical properties, a small weight of $m_w = 54$ g was added to the beam manually before the 40 s mark. The weight was left in place for 5 release tests and removed just before the 60 s mark to return the blade to its nominal state (see Fig. 3).

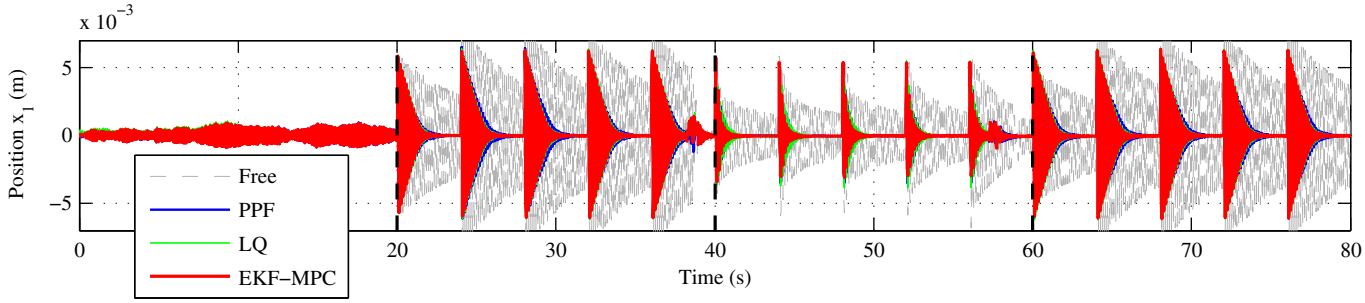

(a) Position of the beam

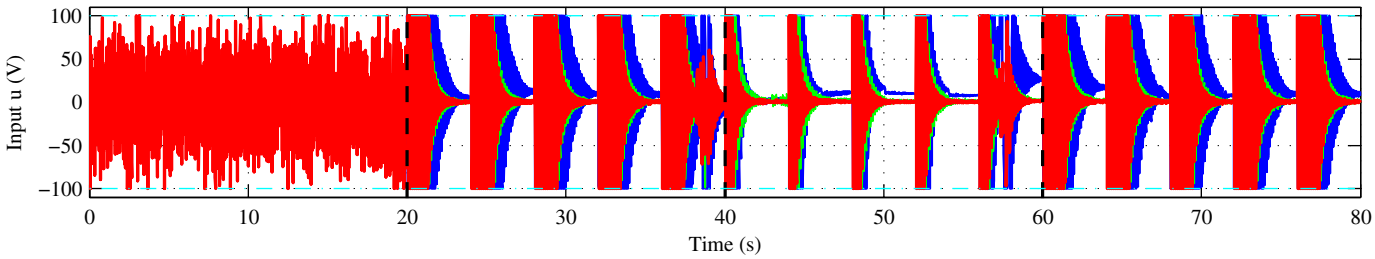

(b) Voltage input to actuators

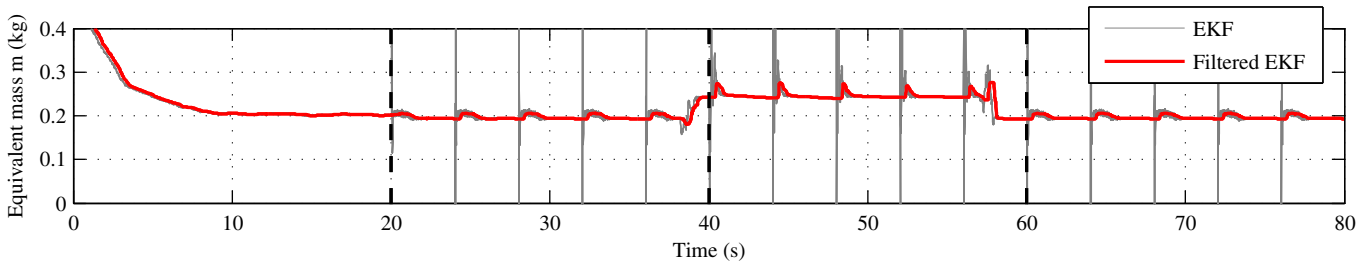

(c) Estimated equivalent mass

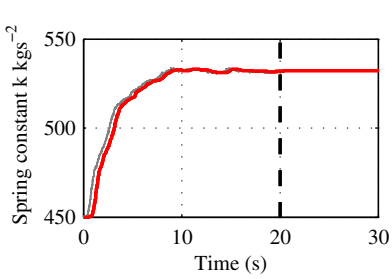

(d) Spring constant estimate

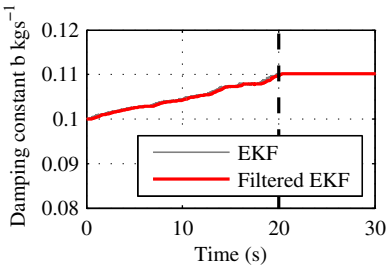

(e) Damping constant estimate

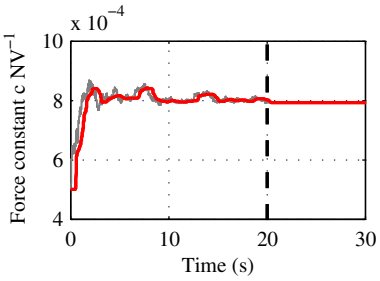

(f) Force conversion constant estimate

Fig. 3. The entire experimental run showing the initial identification procedure (0–20 s), nominal cantilever beam with disturbances (0–40 s and 60–80 s) and the cantilever subjected to a weight change (40–60 s).

4.1 Experiment design and parameters

During the first stage, the system is started up in an initial identification mode with the aim to identify the parameters k,b and c. The actuators are driven by white Gaussian noise and external disturbances are not supplied from the stinger mechanism. At the end of the initial identification phase, the parameters k,b and c are fixed to the latest available value, and the system is switched into control mode with a different EKF setting. The identification EKF was initiated with the initial state estimate $\hat{\boldsymbol{x}}^{+}_{I(0)} = \begin{bmatrix}0 & 0 & 450 & 0.1 & 5\times10^{-4} & 2\end{bmatrix}^T$ and the initial error covariance $\boldsymbol{P}^{+}_{I(0)} = \text{diag}\begin{bmatrix}1\times10^{-5} & 1 & 1\times10^{4} & 1\times10^{-2} & 1\times10^{-6} & 0.1\end{bmatrix}$. With the standard deviation of the position measurement noise of the precision laser system estimated at 1% of 10^{-3} m, the measurement variance was set to $\boldsymbol{R}_I = 1\times10^{-10}$, while the process noise covariance was $\tilde{\boldsymbol{Q}}_{If} = \text{diag}\begin{bmatrix}1\times10^{-4} & 10 & 1\times10^{-5} & 1\times10^{-11} & 1\times10^{-2}\end{bmatrix}$ with $\boldsymbol{Q}_{\theta f} = \tilde{\boldsymbol{Q}}_{\theta f}/T$. All variance values and settings are representative and are estimated based on the physical properties of the controlled system.

The remaining 3 experimental phases ($T_i \geq 20$ s) assumed changes only in the weight of the blade and

the stinger mechanism is engaged to simulate transient vibrations in different closed-loop and an open-loop tests. A different EKF formulation was used (see Sect. 3.1.2), which is initialized with a state estimate $\hat{\boldsymbol{x}}^+_{C0} = [0\ 0\ 2\ 0\ 0]^T$ and initial error covariance $\boldsymbol{P}^+_{C(0)} = \text{diag}\left[1\times10^{-5}\ 1\ 1\times10^{-4}\ 0\ 0\right]$. Compared to the identification phase, measurement noise variance was increased to $\boldsymbol{R}_C = 1\times10^{-6}$, and the process noise covariance was $\tilde{\boldsymbol{Q}}_{Cf} = \text{diag}\left[2\alpha_n(0.63F_e)^2\ 1\times10^2\right]$, where $F_e = 4$ (N) is an estimate of the disturbance force. Tuning parameters of the spectral filter $\omega_n = 2\pi T_e$ and $\alpha_n = 25$ were set empirically to fit the real disturbance, where $T_e = 0.1$ is the estimated duration of the disturbance force. Both the identification and the control EKF used a $dt_I = dt_C = T/500$ s simulation step for the continuous part of the filter.

The MPC part of the adaptive EKF-MPC algorithm uses an $n = 10$ steps prediction horizon with ±100 V constraints on the inputs only. State penalty is set to $\boldsymbol{Q} = \boldsymbol{C}^T\boldsymbol{C}$ and input penalty to $R = 1\times10^{-10}$. The constrained minimization of the quadratic cost function is solved online using the qpOASES quadratic programming solver optimized for MPC use [Ferreau et al., 2008]. The discrete-time linear quadratic controller used in the experimental comparison is computed based on the nominal model with the typical parameters of the blade $m = 0.20$ (kg), $b = 0.11$ (Ns/m), $k = 533$ (N/m) and $c = 8.00\times10^{-4}$ (N/V), which were identified using the same EKF as utilized in the adaptive EKF-MPC algorithm. In order to ensure that the nominal LQ algorithm is tuned analogically to the MPC formulation, the same weights were used for the state and input penalties ($\boldsymbol{Q} = \boldsymbol{C}^T\boldsymbol{C}$, $R = 1\times10^{-10}$).

The positive position feedback controller considered as the second benchmark against the proposed adaptive EKF-MPC algorithm was formulated based on the work of Friswell and Inman [1999], as:

$$\ddot{q}(t) + 2\xi_p\omega_p\dot{q}(t) + \omega_p^2 q(t) = \sqrt{g} \tag{45}$$

$$u(t) = \frac{\sqrt{g}}{c}\omega_p^2 q(t), \tag{46}$$

where ω_p is the natural frequency and ξ_p is the damping ratio of the controller, while g is the gain and the rest were defined in the previous sections. Normally, these parameters are user tunable, however, in the interest of preserving a fair basis of comparison with the proposed vibration controller and nominal LQ, the PPF controller was tuned optimally according to the procedure set forth by Friswell and Inman [1999]. In summary, if the continuous 1 DOF model in Eq. (2) is combined with Eq. (45), then the full output feedback can be expressed as $u(t) = \left[g\omega_p^4\ -\omega_p^2\ -2\xi_p\omega_p\right]\boldsymbol{y}_p$, where $\boldsymbol{y}_p$ is the output of the state-space system augmented by the PPF controller. This feedback gain and subsequently all the parameters of the original PPF controller can be computed optimally, if a continuous infinite-horizon quadratic cost function is minimized with the PPF augmented state-space model and weights Q_p and P_p:

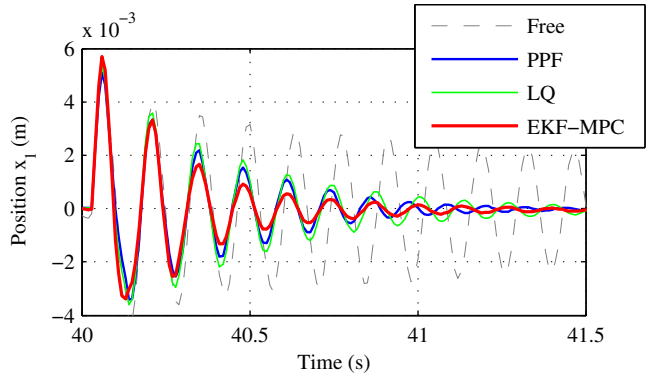

(a) Output detail (position)

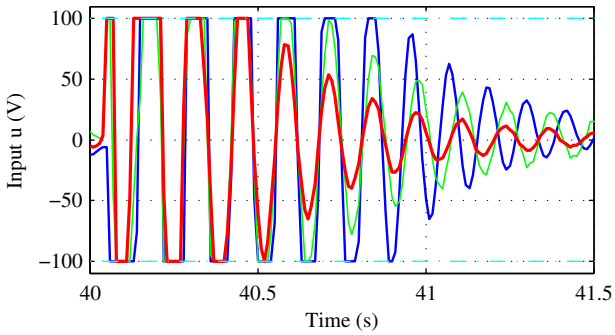

(b) Input detail (voltage)

Fig. 4. Detail of the position and the corresponding voltage input for the system subjected to a weight change and transient impact disturbance

$$\boldsymbol{Q_p} = \begin{bmatrix}\alpha & 0 & 0\\ 0 & \frac{1}{c^2}\beta & 0\\ 0 & 0 & \frac{1}{c^2}\gamma\end{bmatrix} \qquad \boldsymbol{R_p} = R_p = \frac{1}{c^2}\delta. \tag{47}$$

The optimization procedure above was performed with the physical parameters identical to the ones used with the nominal LQ controller. To ensure a maximal agreement of PPF and LQ performance, the tuning parameters were chosen as $\beta = 0$, $\gamma = 0$ and $\delta = R = 1\times10^{-10}$, while the only remaining parameter $\alpha = 1.7\times10^8$ was chosen empirically to ensure that the difference between nominal PPF and LQ output performance remained minimal.

All experiments were sampled by $T = 0.01$ s. The input side of the measurement chain included a low-pass filter with a pass band edge at 30 Hz and a stop band edge at 50 Hz. The input was also filtered using a windowed running mean filter with a 0.1 Hz fundamental frequency, in order to remove the static deformation component of the beam position. To remove the sudden changes in estimated weight caused by the impacts to the beam, the weight estimates were filtered using a running windowed median filter with a 50 sample width and a 49 sample buffer overlap. The filtered estimates were used to update the continuous model and discretized using $j = 10$ approximations. The constraints on the inputs are enforced using saturation limits in the case of the nominal LQ and PPF controllers.

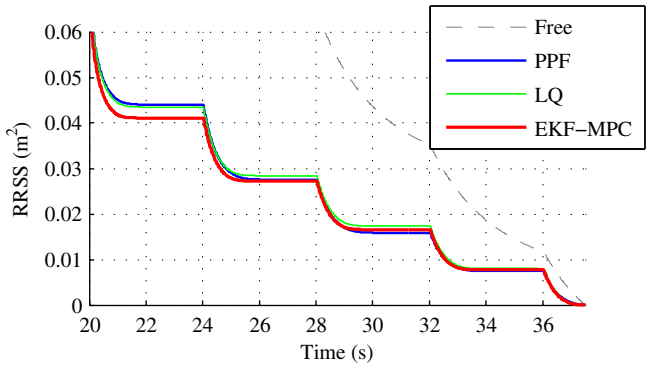

(a) RRSS for output

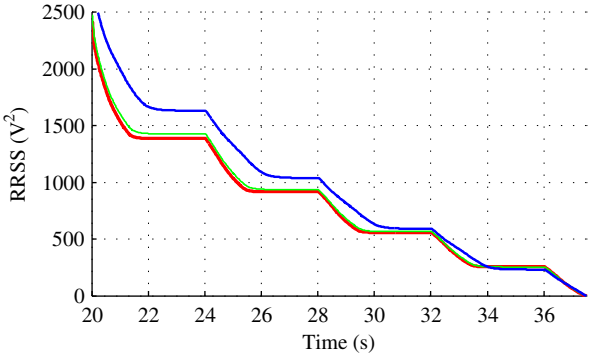

(b) RRSS for input

Fig. 5. Remaining root of sum of squares performance indicator for the nominal system

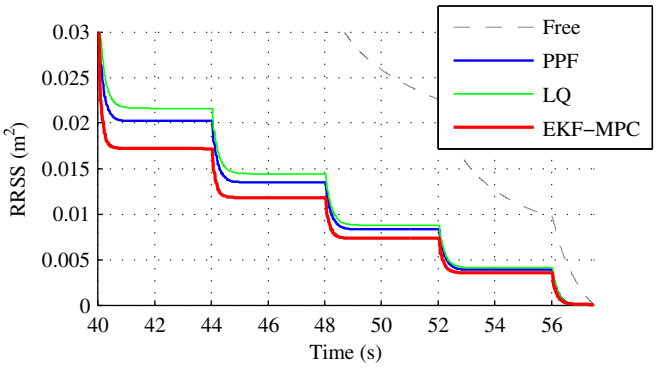

(a) RRSS for output

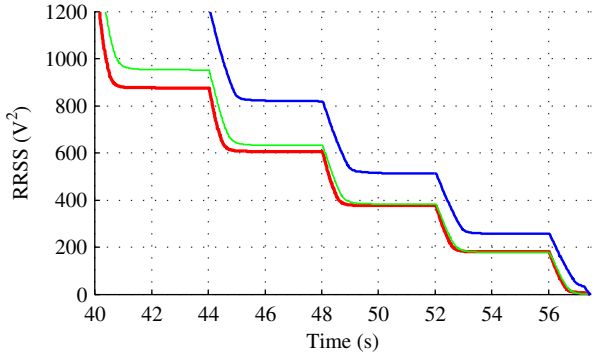

(b) RRSS for input

Fig. 6. Remaining root of sum of squares performance indicator for the system subjected to a weight change

4.2 Experimental results

The results for all experimental stages and scenarios are shown in Fig. 3, including the position (Fig. 3(a)), voltage input (Fig. 3(b)), direct and filtered weight estimates (Fig. 3(c)) and the parameters that are identified only in the first stage of the experiment (Fig.3(d)–3(f)). From these, it is clear that all closed-loop controllers provide significantly better damping performance than the open-loop response of the blade. The performance difference of the investigated controllers is more subtle, except that the PPF controller requires significantly more input to achieve a comparable result (see Fig. 3(b)). After the initial estimation of all physical parameters the estimated equivalent mass reacts to the sudden changes caused by the impacts of the stinger mechanism, then adapts to the weight added to and subsequently removed from the beam. Note that even though the increase in weight is in correspondence with the real physical weight change, this is a dynamically equivalent estimate, which depends largely on the placement of the mass on the blade.

The difference between the proposed vibration control method, nominal LQ and nominal PPF is visually more distinguishable in Fig. 4, showing a single 1.5 s long transient vibration response in case the weight of the blade is altered (Stage 3, 40–60 s). The outputs in Fig. 4(a) suggest, that the best performance is to be expected from the adaptive EKF-MPC controller which adapts to the change, while though nominal PPF seems to have a little advantage over LQ, both perform worse than the proposed method. Even though their tuning is analogous, this performance difference is achieved with the least control effort from the adaptive EKF-MPC controller, with the nominal LQ supplying considerably more inputs to the actuators (Fig. 4(b)). While PPF provides better results than LQ in comparison, it needs more effort to achieve this.

To complement this visual comparison with objective indicators, the performance of the individual controllers was evaluated numerically using the root of sum of squares (RSS) criterion for the output deviation and input deviation from equilibrium. Since the difference between algorithm performance can be often masked if the system response oscillates, the performance is also visualized here using the remaining root of sum of square (RRSS) criterion defined as

$$RRSS(k) = \sqrt{\sum_{i=0}^{T_f} e_i^2} - \sqrt{\sum_{i=0}^{k} e_i^2} \tag{48}$$

where the first part of the equation on the left is RSS, T_f is the length of the experiment in samples, e_i is the error for a given time step for both the output $e_i = y_{\text{ref}} - y_{(i)} = 0 - y_{(i)}$ and the input $e_i = 0 - u_{(i)}$.

The RSS criterion was computed for the nominal blade configuration in between 20–37.5 s for all scenarios. In case the performance of the proposed adaptive EKF-MPC controller is taken as the basis of comparison (100%), a larger result indicates worse output performance and more control effort. The performance difference visible in the

output and input is confirmed by these indicators and their visualization by the RRSS criterion in Fig. 5. Given a saturated LQ controller is tuned identically to constrained MPC, there is still an slight performance loss. The tuning of the PPF controller matches LQ within 3%, but this is achieved by a substantially increased output activity. The difference between closed- and open-loop control is larger than a factor of 5.

RSS performance indicators (nominal system)				
	EKF-MPC	LQ	PPF	Free
Position x_1(%)	100*	110	107	567
Input u(%)	100*	104	144	—

*=Base value.

Similarly to the formerly presented nominal RSS comparison, the indicators were calculated again for the time period of 40–57.5 s, that is, the case when the blade mass was altered (see also Fig. 6). The performance difference is now more pronounced, with the adaptive EKF-MPC controller providing the highest degree of damping, followed by the PPF and finally the LQ controller. The extent of effort mirrored by the level of input voltages corresponds to the earlier discussion: the LQ controller requires an increased amount of input moves to achieve worse results than adaptive EKF-MPC, while the increment in input PPF activity is quite striking.

RSS performance indicators (weight change)				
	EKF-MPC	LQ	PPF	Free
Position x_1 (%)	100*	142	120	742
Input u (%)	100*	124	189	—

*=Base value.

5. CONCLUSION

This article proposes the use of an adaptive predictive controller with joint state and weight parameter estimation to increase the damping of transient vibrations in structures resembling cantilever beams with variable weight. The vibration controller set forth in this paper is a combination of the extended Kalman filter augmented by the unknown equivalent mass parameter and dual-mode constrained model predictive control. The performance of the controller is evaluated experimentally and compared to long-established methods used for the active control of transient vibrations. The experimental results and the following discussion suggest that, even though all reasonable effort is made to tune the LQ and PPF controllers analogously to MPC, the performance of the proposed adaptive EKF-MPC controller surpassed these traditional methods—mainly because of its adaptive features. Moreover, this was achieved with less inputs supplied to the actuators, meaning a potential increase in the life-expectancy of the actuators and less strain on the controlled structure.

REFERENCES

S. B. Choi, Y. K. Park, and T. Fukuda. A proof-of-concept investigation on active vibration control of hybrid smart structures. *Mechatronics*, 8(6):673–689, 1998.

H. J. Ferreau, H. G. Bock, and M. Diehl. An online active set strategy to overcome the limitations of explicit MPC. *Int J Robust Nonlin*, 18(8):816–830, 2008.

G. F. Franklin, J. D. Powell, and M. L. Workman. *Digital Control of Dynamic Systems*. Addison-Wesley, Boston, MA, 3. edition, 1997.

M. I. Friswell and D. J. Inman. The relationship between positive position feedback and output feedback controllers. *Smart Mater Struct*, 8(3):285, 1999.

Y. R. Hu and A. Ng. Active robust vibration control of flexible structures. *J Sound Vib*, 288(1–2):43–56, 2005.

D. J. Inman. *Vibration with control*. John Wiley & Sons, Chichester, England, 2006.

E. Lourens, E. Reynders, G. De Roeck, G. Degrande, and G. Lombaert. An augmented Kalman filter for force identification in structural dynamics. *Mech Syst Signal Pr*, 27(0):446–460, 2012.

J. M. Maciejowski. *Predictive Control with Constraints*. Prentice Hall, Upper Saddle River, NJ, September 2000.

P. S. Maybeck. *Stochastic Models, Estimation and Control*. Academic Press, New York,NY, 1. edition, 1979.

T.F. Mu, L. Zhou, and J.N. Yang. Adaptive extended Kalman filter for parameter tracking of base-isolated structure under unknown seismic input. In *10th International Bhurban Conference on Applied Sciences and Technology (IBCAST)*, pages 84–88, 2013.

T. Pappas, A.J. Laub, and N. R. Sandell. On the numerical solution of the discrete-time algebraic Riccati equation. *IEEE T Automat Contr*, 25(4):631–641, 1980.

J. Richelot, J. Bordeneuve-Guibe, and V. Pommier-Budinger. Active control of a clamped beam equipped with piezoelectric actuator and sensor using generalized predictive control. In *2004 IEEE International Symposium on Industrial Electronics*, pages 583 – 588, 2004.

J. A. Rossiter. *Model-Based Predictive Control: A Practical Approach*. CRC Press, Boca Raton, FL, 2003.

P. O. M. Scokaert and J. B. Rawlings. Infinite horizon linear quadratic control with constraints. In *Proceedings of IFAC'96 World Congress*, volume 7a-04 1, pages 109–114, San Francisco, 1996.

D. Simon. *Optimal State Estimation: Kalman, H_∞, and Nonlinear Approaches*. Wiley–Interscience, Hoboken,NJ, 2006.

G. Song, S. P. Schmidt, and B. N. Agrawal. Experimental robustness study of positive position feedback control for active vibration suppression. *J Guid Control Dynam*, 25 (1):179–182, 2002.

K. Szabat and T. Orlowska-Kowalska. Application of the extended Kalman filter in advanced control structure of a drive system with elastic joint. In *IEEE International Conference on Industrial Technology, 2008.*, pages 1–6, 2008.

T. Nestorovic Trajkov, H. Koppe, and U. Gabbert. Direct model reference adaptive control (MRAC) design and simulation for the vibration suppression of piezoelectric smart structures. *Commun Nonlinear Sci Numer Simulat*, 13(9):1896 – 1909, 2008.

A. Unger, F. Schimmack, B. Lohmann, and R. Schwarz. Application of LQ-based semi-active suspension control in a vehicle. *Control Eng Pract*, (0):–, 2013. In press.

C. M. A. Vasques and J. Dias Rodrigues. Active vibration control of smart piezoelectric beams: Comparison of classical and optimal feedback control strategies. *Computers & Structures*, 84(22-23):1402 – 1414, 2006.

T. Zhang, H. G. Li, and G. P. Cai. Hysteresis identification and adaptive vibration control for a smart cantilever beam by a piezoelectric actuator. *Sensor Actuat A-Phys*, 203(0):168–175, 2013.